AIAA SciTech Forum
11–15 & 19–21 January 2021, Virtual Event
AIAA SciTech 2021 Forum

Maneuver Load Alleviation of Very Flexible Aircraft via Nonlinear Decoupling Control

Molong Duan*, Ilya V. Kolmanovsky†, and Carlos E. S. Cesnik‡
University of Michigan, Ann Arbor, Michigan, 48109, USA

With the pursuit of operating cost and emission reductions, modern transport aircraft increasingly adopt designs with high-aspect-ratio wings and lightweight structures. Accordingly, to avoid structural failure, the flight control system of very flexible aircraft is expected to alleviate the structural loads besides its standard function of rigid-body trajectory tracking. For very flexible aircraft with redundant control effectors, these two objectives can be addressed in a decoupled way by exploiting input redundancy. This paper proposes a maneuver load alleviation method exploiting nonlinear aircraft models and nonlinear decoupling control. The proposed method generates a time-varying open-loop signal to augment an existing flight controller and provide load alleviation function. The proposed method is verified in simulations on a general transport aircraft and on an X-HALE aircraft, showing that the flexible outputs can be made to satisfy the prescribed bounds without changing the rigid-body responses during a maneuver.

I. Introduction

High-aspect-ratio wings and lightweight materials are increasingly used in modern aircraft design to enhance fuel efficiency. This trend naturally increases the structural flexibility of the aircraft. The very flexible aircraft (VFA) design, despite the benefit of fuel efficiency, is more susceptible to over stress, leading to potential structural failure under aggressive maneuvers or gust. Therefore, the control system of VFA is expected to take both rigid-body dynamics and structural dynamics into consideration, providing the additional function of load alleviation. With the increased aspect ratio and flexibility, the traditional controllers which use notch filters to avoid exciting structural modes are no longer sufficient [1, 2]. Also, additional control effectors (wing tip devices [3, 4], variable camber flap [5], etc.) are introduced for the purpose of alleviating loads, which requires more systematic coordination and optimization from the flight controller.

Most existing control-based maneuver load alleviation (MLA) approaches strive to distribute the control actions among the control effectors (including the elevators, ailerons, flaps, and thrust inputs) in a way that the structural loads are minimized or confined within given bounds. Early designs of MLA systems symmetrically deflected the wing control surfaces based on aircraft normal acceleration to reduce structural loads [6]. This approach changes the spanwise lift distribution such that the bending moment at the root of the wing is reduced. However, the effect of MLA functionality on the rigid-body tracking performance is not explicitly considered. To more extensively consider the balance of the MLA functionality and the rigid-body trajectory tracking, Burlion et al. [7] proposed an $\mathcal{H}_\infty$ approach with an output saturation strategy to balance objectives of the flight tracking performance and wing root bending moment clearance. Hashemi and Nguyen [8] proposed a two-stage model reference adaptive control method, including a primary objective of rigid-body tracking and a secondary objective of MLA. Also, model predictive control approaches [9, 10] are introduced in a way that both the rigid-body tracking and MLA are included in the optimization objective or constraint formulations.

The increased level of input redundancy in modern aircraft provides additional opportunities to achieve MLA. For static responses, Zink et al. [11] and Raveh [12] proposed methods to optimize the trim solutions of input redundant aircraft considering the additional objective of minimizing root bending moment. In addition, the input redundancy is exploited to provide a more systematic solution to balance the dynamics of the rigid-body responses and the MLA functionality. Frost et al. [13] developed a control allocation framework for input redundant aircraft considering the structural load feedback. Gaulocher et al. [14] explicitly explored a way to decouple the structural load alleviation and trajectory tracking of input redundant aircraft within the model predictive control framework. Hansen et al. [15, 16]

*Research Fellow, Department of Aerospace Engineering, molong@umich.edu.
†Professor, Department of Aerospace Engineering, AIAA Member, ilya@umich.edu.
‡Clarence L. (Kelly) Johnson Professor, Department of Aerospace Engineering, AIAA Fellow, cesnik@umich.edu.

established a dynamic null space filter for the rigid-body states and achieved the load alleviation without impacting the rigid-body responses. However, most existing MLA methods exploiting input redundancy assume a linear aircraft model, which may be restrictive since large deformations of VFA may introduce significant nonlinearities [17].

In this work, an MLA method for nonlinear input redundant VFA is proposed. The proposed method exploits the properties of input redundancy [18] in a way that the rigid-body responses are kept unchanged while the flexible states are modified to satisfy given structural bounds. The proposed method exploits the nonlinear decoupling control theory applied to nonlinear VFA models and generates the time-varying feedforward control signals for the redundant control effectors to be used during the maneuver. Therefore, this approach is compatible with existing aircraft controllers.

The paper is organized as follows. The background on the nonlinear decoupling control principle is introduced in Section II. The definitions of input redundant VFA and the corresponding MLA method exploiting input redundancy is detailed in Section III. The simulation case studies for a general transport aircraft [19, 20] and a very flexible X-HALE aircraft [21] are shown and discussed in Section IV.

II. Background on Nonlinear System Input-Output Decoupling

Consider a nonlinear system with the state $x \in \mathbb{R}^{n_x}$, the output $y \in \mathbb{R}^{n_y}$, and the control input $u \in \mathbb{R}^{n_u}$ in the form of

$$\begin{aligned} \dot{x} &= f(x) + g(x)u, \\ y &= h(x), \end{aligned} \tag{1}$$

where $f(x) : \mathbb{R}^{n_x} \to \mathbb{R}^{n_x}$, $g(x) = [g_1(x), ..., g_{n_u}(x)] : \mathbb{R}^{n_x} \to \mathbb{R}^{n_x \times n_u}$, and $h(x) = \{h_1(x), ..., h_{n_y}(x)\}^\top : \mathbb{R}^{n_x} \to \mathbb{R}^{n_y}$ are nonlinear functions satisfying appropriate smoothness assumptions. The input-output decoupling of such a nonlinear system (*i.e.*, Morgan's problem [22]) involves finding nonlinear functions $\alpha(x) : \mathbb{R}^{n_x} \to \mathbb{R}^{n_u}$ and $\beta(x) : \mathbb{R}^{n_x} \to \mathbb{R}^{n_u \times n_u}$, such that a state feedback controller in the form of

$$u = \alpha(x) + \beta(x)v, \ v \in \mathbb{R}^{n_u}, \tag{2}$$

leads to each channel of v_i, $i = 1, \cdots, n_y$, only controlling y_i and not affecting y_j when $i \neq j$.

In the solution of the input-output decoupling problem, the system's relative degree vector $\rho \in \mathbb{N}^{n_y}$ is defined in a neighborhood $U(x_0)$ of a given state x_0 as

$$\rho = \{\rho_1, \rho_2, ..., \rho_{n_y}\}^\top, \tag{3}$$

satisfying

$$\begin{cases} L_g L_f^k h_j(x) = 0, x \in U(x_0), k < \rho_j - 1, \\ L_g L_f^{\rho_j - 1} h_j(x_0) \neq 0. \end{cases} \tag{4}$$

Here L_f^k denotes the kth order Lie derivative of a function with respect to f; L_g denotes the Lie derivative of a function with respect to g. With a well-defined relative degree vector, an $n_y \times n_u$-dimensional decoupling matrix $D(x) = [d_{ij}(x)]$ and an n_y-dimensional decoupling vector $b(x) = \{b_i(x)\}$ are defined as

$$d_{ij}(x) = L_{g_j} L_f^{\rho_i - 1} h_i(x), \ i = 1, ..., n_y, \ j = 1, ..., n_u, \tag{5}$$

$$b_i(x) = L_f^{\rho_i} h_i(x), \ i = 1, ..., n_y. \tag{6}$$

Note that the decoupling matrix $D(x)$ and vector $b(x)$ connect to the derivatives of the output with given relationship

$$\begin{Bmatrix} y^{(\rho_1)} \\ \vdots \\ y^{(\rho_{n_y})} \end{Bmatrix} = D(x)u + b(x). \tag{7}$$

Asymptotic tracking for nonlinear systems with more inputs than outputs has been considered, *e.g.*, in [23]. For a system with $n_u \geq n_y$, the input-output decoupling problem is solvable if and only if the decoupling matrix $D(x)$ has rank n_y [22]. When this condition is satisfied, $D(x)$ can be decomposed, without loss of generality, as

$$D(x) = [D_1(x), D_2(x)], \tag{8}$$

where $D_1(x)$ is a $n_y \times n_y$-dimensional non-singular square matrix, and $D(x)$ can be transformed to $[D_1(x), 0]$ through column elimination. Without loss of generality, the column elimination transformation is represented by an $n_u \times n_u$-dimensional non-singular transformation matrix $\beta_1(x)$ such that

$$D(x)\beta_1(x) = [D_1(x), 0]. \tag{9}$$

With this decomposition and transformation, a straightforward solution to the input-output decoupling problem is given by

$$\alpha(x) = -\beta_1(x) \begin{bmatrix} D_1^{-1}(x)b(x) \\ 0_{n_u - n_y} \end{bmatrix}, \tag{10}$$

$$\beta(x) = \beta_1(x) \begin{bmatrix} D_1^{-1}(x) & 0 \\ 0 & I_{n_u - n_y} \end{bmatrix}. \tag{11}$$

In cases where the dimensions of the input and output are matched (*i.e.*, $n_u = n_y$), $\beta_1(x) = I$ and $D(x) = D_1(x)$. With the feedback law in Eqs. (2), (10), and (11), *i.e.*,

$$y^{(\rho_i)} = v_i, \ i = 1, \cdots, n_y, \tag{12}$$

The additional channels of v (*i.e.*, $v_{n_y+1}, ...v_{n_u}$) can be chosen freely without affecting the selected outputs. The computation of an open loop (feedforward) control for MLA can benefit from the decoupling transformation given by Eqs. (2), (10), and (11).

III. Maneuver Load Alleviation Exploiting Nonlinear Input-Output Decoupling

A. Very Flexible Aircraft and Input Redundancy

Consider a very flexible aircraft with n_u control inputs, including all the control surfaces and thrusters. A nonlinear flight dynamics model G is given by

$$\begin{aligned} \dot{x} &= f(x) + \sum_{i=1}^{n_u} g_i(x)u_i, \\ y &= \begin{Bmatrix} y_r \\ y_f \end{Bmatrix} = \begin{Bmatrix} h_r(x) \\ h_f(x) \end{Bmatrix}, \end{aligned} \tag{13}$$

where the output y is decomposed into a vector representing the rigid-body motion $y_r \in \mathbb{R}^{n_r}$ and a vector representing structural deformation $y_f \in \mathbb{R}^{n_f}$; $h_r(x)$ and $h_f(x)$ are the corresponding nonlinear functions mapping the state x to y_r and y_f. The dimension of the output satisfies $n_y = n_r + n_f$. It is assumed that the system has no feed-through terms directly from inputs to outputs, which which is the case for aircraft models we subsequently consider. The rigid-body output y_r typically includes the translational velocities, rotational velocities, orientation angles, etc. The flexible output y_r is typically chosen to be the curvature, bending moment, or load factor at the critical stations on the aircraft.

Modern aircraft are usually equipped with redundant control effectors to enhance their fault tolerance. This redundancy can be categorized into two types, *i.e.*, strong input redundancy or weak input redundancy. Strong input redundancy usually arises when there are more inputs than the states ($n_u > n_x$). It is characterized by the existence of a nontrivial null space of $g(x)$, *i.e.*,

$$\text{Ker}\,(g(x)) \neq 0, \ \forall x \in X \subseteq \mathbb{R}^{n_x}, \tag{14}$$

where X is the set of all admissible states x. Strong input redundancy is typically exploited for the control of rigid aircraft in the form of direct inversion, control allocation, etc. However, these control methods for strong input redundancy cannot be readily applied to VFA due to the large number of elastic states. When $n_x \gg n_u$, the condition for strong input redundancy (*i.e.*, Eq. (14)) typically does not hold. Therefore, for VFA, weak input redundancy [24] defined by input-output properties is more applicable. The system in Eq. (13) is said to exhibit weak input redundancy if the $D(x)$ matrix in Eq. (5) has a nontrivial null space, *i.e.*,

$$\text{Ker}\,(D(x)) \neq 0, \ \forall x \in X \subseteq \mathbb{R}^{n_x}. \tag{15}$$

Note that the dimension of $D(x)$ is determined by the number of the inputs and the outputs, therefore, the property of weak input redundancy also depends on the outputs selected. In this work, we assume the aircraft is weakly input redundant if there exist more control effectors than the rigid-body outputs to be controlled (*i.e.*, $n_u > n_r$). Also, we assume the number of flexible outputs to be controlled satisfy the relationship $n_f \leq n_u - n_r$ such that the condition for the input-output decoupling problem to be solvable (*i.e.*, the rank of $D(x)$ equals n_y) is not violated. This assumption indicates that the number of flexible modes that the proposed method is capable of handling increases with the number of inputs.

B. Maneuver Load Alleviation Exploiting Input Redundancy and Input-Output Decoupling

The control or VFA is expected to achieve two main goals. Firstly, the aircraft is supposed to track a given flight trajectory, which is typically achieved through the feedback control using the rigid-body outputs y_r. Secondly, in the context of VFA, the structural loads at critical stations on the aircraft (*i.e.*, y_f) are expected to be kept within specified limits to satisfy structural integrity requirements. This secondary control objective is referred to as load alleviation. Note that the assumption of weak input redundancy of VFA (*i.e.*, $n_u > n_r$) provides an opportunity to separate the two objectives. In particular, there exist multiple control input trajectories $u(t)$ that yield the same rigid-body trajectories $y_r(t)$. Therefore, the control effort can be redistributed among the control effectors to achieve both the specified trajectory tracking and load alleviation. Out of the two major sources of in-flight structural loads (*i.e.*, maneuver and gust), this work focuses on maneuver load alleviation. The detailed procedure exploiting the input redundancy is illustrated in Figure 1.

Assume that the vector of rigid-body outputs y_r is expected to track a nominal reference r and this tracking is performed by a nominal feedback tracking controller C with the control signal it generates denoted by u_0. This nominal controller C can be either linear or nonlinear, and it only uses the rigid-body outputs for feedback. The control signal u_0 is augmented, in advance of the maneuver, by another control signal Δu, which is generated through a load alleviation function. The load alleviation function takes the reference, predicted nominal control signal u_0, load bounds, and nonlinear dynamics of VFA into consideration, yielding a control input Δu adding to the nominal control u_0. In our approach, which is further explained below, this modification Δu is computed as a time-dependent feedforward signal over a specified preview horizon and in advance of the maneuver, under the assumption that the preview of the reference r is available. The control signal modification is informed so that Δu causes no or minimal changes to the rigid-body output y_r while ensuring that the flexible outputs y_f are within their desired lower and upper bounds y_f^- and y_f^+, respectively. In this way, the two objectives of tracking and load alleviation are decoupled. Note that the load alleviation block input and output signals are represented by a dotted lines in Figure 1, signifying that the computation of Δu is performed in advance of the maneuver while once Δu is computed, it is applied as a time-dependent open-loop/feedforward input to the system during the actual maneuver wherein the nominal controller C generates u_0 based on feedback. In this way, trajectory tracking is decoupled from load alleviation.

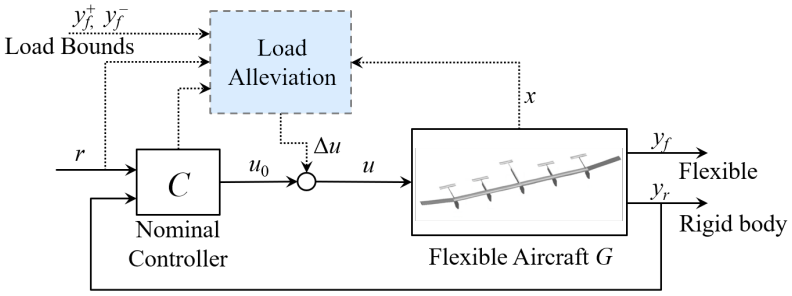

Fig. 1 Block diagram of maneuver load alleviation with nominal controller

To implement the load alleviation approach, the ability to forecast the trajectory of the state x over the preview horizon is necessary. In this work, it is assumed that a reduced-order nonlinear model of the VFA G is available, and its state x is accurately estimated. the nonlinear model of the VFA G is a reduced-order model and the state x is accurately measured/estimated. The reduced dimension n_x is typically around 10 to 20, in contrast to the original VFA model with thousands of states.

We now consider the computation of Δu for load alleviation in detail. Suppose that the reference trajectory $r(t)$,

$t \in [0, T]$ for rigid-body outputs has been specified as a time function in advance of the maneuver. The starting time is specified as 0 without loss of generality; T is specified as the end time of the entire maneuver. Assume the nominal controller C has already been designed and the tracking performance is satisfactory. This nominal controller C is assumed to take only the reference r and the rigid-body output y_r to generate the nominal control signal. It is represented by

$$\begin{aligned} \dot{x}_c &= f_c(x_c) + g_{cy}(x_c)y_r + g_{cr}(x_c)r, \\ u_0 &= h_c(x_c) + h_{cy}(x_c)y_r + h_{cr}(x_c)r, \end{aligned} \tag{16}$$

where x_c is the vector of the controller states, and f_c, g_{cy}, g_{cr}, h_c, h_{cy}, and h_{cr} are functions of x_c. With the given initial system state $x(0)$ and the controller state $x_c(0)$, the controller input $u_0(t)$ and the output $y(t)$ during the maneuver time interval $[0, T]$ can be predicted using the numerical simulation of the nonlinear model G in Eq. (13) and the controller C in Eq. (16). The corresponding control signal and output are written as $\hat{u}_0(t)$ and $\hat{y} = \{\hat{y}_r^\top(t), \hat{y}_f^\top(t)\}^\top$, respectively. Given the decoupling relation given by Eqs. (2), (10), (11), and (12), the time history of the pseudo-input $\hat{v}(t)$ can be derived to satisfy the following relationship

$$\begin{bmatrix} \hat{y}_1^{(\rho_1)} \\ \hat{y}_2^{(\rho_2)} \\ \vdots \\ \hat{y}_{n_y}^{(\rho_{n_y})} \end{bmatrix} = D(\hat{x})\hat{u}_0 + b(\hat{x}) = \begin{bmatrix} I_{n_y} & 0 \end{bmatrix} \hat{v}, \tag{17}$$

where $\hat{y}_i^{(\rho_i)}$, $i = 1, ..., n_y$, denotes the ρ_i-order time derivative of $\hat{y}_i$. Using Eq. (17), the first n_y elements in $\hat{v}$ can be calculated, as functions of time, through the differentiation of the predicted output $\hat{y}$, while the last $n_u - n_y$ elements of $\hat{v}$ remain to be defined. Assume the vectors of the lower and upper bounds on the corresponding flexible outputs are given by y_f^- and y_f^+, the pseudo-input is partitioned as

$$\hat{v} = \begin{bmatrix} \hat{v}_r \\ \hat{v}_{f1} \\ \hat{v}_{f2} \end{bmatrix}, \tag{18}$$

where $\hat{v}_r \in \mathbb{R}^{n_r}$ corresponds to the rigid-body output; $\hat{v}_{f1}$ corresponds to the set of flexible outputs (defined as y_{f1}) for which the bounds (specified as y_{f1}^- and y_{f1}^+) are exceeded based on the nominal prediction; $\hat{v}_{f2}$ corresponds to the set of flexible outputs (defined as y_{f2}) for which the bounds (specified as y_{f2}^- and y_{f2}^+) are satisfied. Note that without loss of generality, the outputs with bound violations are assumed to be the first n_{f1} flexible states in Eq. (18).

Define $\bar{y}_{f1}$ as the constrained $\hat{y}_{f1}$ as

$$\bar{y}_{f1,i}(t) = \begin{cases} y_{f1,i}^-, \text{when } \hat{y}_{f1,i}(t) < y_{f1,i}^- \\ y_{f1,i}^+, \text{when } \hat{y}_{f1,i}(t) > y_{f1,i}^+ \\ \hat{y}_{f1,i}(t), \text{otherwise} \end{cases}, \; i = 1, ..., n_{f1}, \tag{19}$$

where $\hat{y}_{f1,i}(t)$ is ith element of $\hat{y}_{f1}(t)$ (same notation applies to y_{f1}^-, y_{f1}^+, and $\bar{y}_{f1}(t)$). Although $\bar{y}_{f1}(t)$ satisfies the constraints, it needs to be approximated by a sufficiently smooth function to be used in Eq. (17). Assume $\tilde{y}_{f1}(t)$ is a sufficiently smooth approximation of $\bar{y}_{f1}(t)$ that guarantees continuity of the output differentiated up to its relative degree while satisfying the constraints. Each element of the modified $\tilde{v}_{f1}$ is defined as

$$\tilde{v}_{f1,i} = \tilde{y}_{f1,i}^{(\rho_{i+n_r})}, \; i = 1, ..., n_{f1}. \tag{20}$$

Let

$$\tilde{v}(t) = \begin{bmatrix} \tilde{v}_r(t) \\ \tilde{v}_{f1}(t) \\ \tilde{v}_{f2}(t) \end{bmatrix}, \tag{21}$$

and $\tilde{v}_r = \hat{v}_r$. Note that $\tilde{v}_{f2}$ in Eq. (21) remains still to be defined. Due to the decoupling design properties, these degrees of freedom can be used to satisfy additional control objectives without affecting the rigid-body tracking and

load alleviation. Note that typically it is desirable that the load alleviation function minimally alters the nominal control u_0. With $\tilde{v}_r$ and $\tilde{v}_{f1}$ specified, $\tilde{v}_{f2}$ can be computed by solving the following optimization problem,

$$\min_{\tilde{v}_{f2}(t)} \left\| \tilde{u}(\tilde{v}_r(t), \tilde{v}_{f1}(t), \tilde{v}_{f2}(t), \tilde{x}(t)) - \hat{u}_0(t) \right\|_2^2, \tag{22}$$

at each time instant t, $0 \le t \le T$, where $\tilde{x}$ and $\tilde{u}$ are the corresponding state and control signals in the simulation with $\tilde{v}(t)$, respectively. Note that we can represent $\tilde{u}$ in the form of

$$\tilde{u} = \alpha(\tilde{x}) + \beta_{r,f1}(\tilde{x}) \begin{bmatrix} \tilde{v}_r \\ \tilde{v}_{f1} \end{bmatrix} + \beta_{f2}(\tilde{x})\tilde{v}_{f2}, \tag{23}$$

where $\beta_{r,f1}(x) \in \mathbb{R}^{n_u \times (n_r + n_{f1})}$ and $\beta_{f2}(x) \in \mathbb{R}^{n_u \times n_{f2}}$ are the decomposition of $\beta(x)$, *i.e.*,

$$\beta(x) = \begin{bmatrix} \beta_{r,f1}(x) & \beta_{f2}(x) \end{bmatrix}. \tag{24}$$

Then the minimization in Eq. (22) yields

$$\tilde{v}_{f2}(t) = \beta_{f2}^{+}(\tilde{x}(t)) \left(\hat{u}_0(t) - \alpha(\tilde{x}(t)) - \beta_{r,f1}(\tilde{x}(t)) \begin{bmatrix} \tilde{v}_r(t) \\ \tilde{v}_{f1}(t) \end{bmatrix} \right), \tag{25}$$

where $\beta_{f2}^{+}(\tilde{x})$ is the pseudoinverse of $\beta_{f2}(\tilde{x})$. The detailed procedure of the entire load alleviation function is summarized in Figure 2. The shaded areas indicate the two rounds of the required time-domain simulation. The first simulation determines $\hat{u}_0(t)$ and $\hat{y}(t)$ while the second simulation determines $\tilde{u}(t)$. The dotted lines indicate that the entire time history of the signal is used in the processing.

With this $\tilde{v}(t)$ only the flexible response is modified, and the corresponding control signal is given by

$$\tilde{u}(t) = \alpha(\tilde{x}(t)) + \beta(\tilde{x}(t))\tilde{v}(t), \ 0 \le t \le T, \tag{26}$$

where $\tilde{x}(t)$ is the state trajectory simulated using this modified decoupling control with the system dynamics in Eq. (13). This $\tilde{u}(t)$ represents the control input trajectory which preserves the rigid-body trajectory and provides MLA. Finally,

$$\Delta u(t) = \tilde{u}(t) - \hat{u}_0(t), \ 0 \le t \le T, \tag{27}$$

is the open-loop modification applied as a time-varying feedforward during the maneuver to augment the control signal generated by the nominal feedback controller in response to the actual rigid-body output measurements during the maneuver. Note that the decoupling-based design greatly simplifies the generation of MLA control signals as $\Delta u(t)$ does not affect the rigid-body outputs and the nominal controller output u_0.

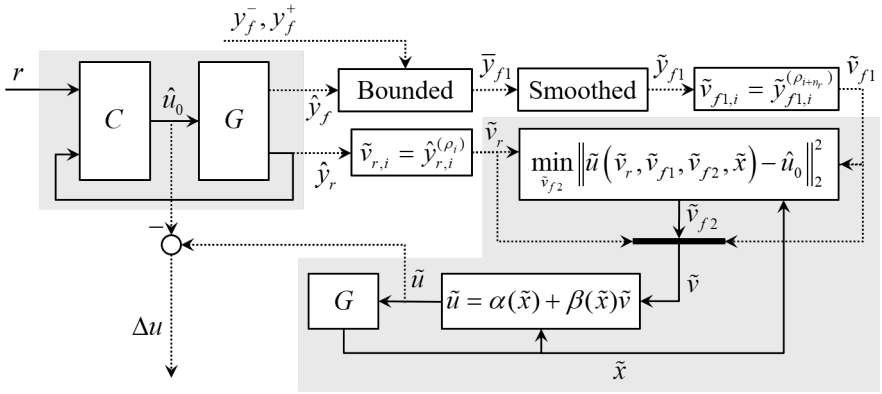

Fig. 2 Block diagram of load alleviation function

IV. Simulation Case Studies

The new MLA method based on input-output decoupling is verified with a general transport aircraft (GTA) [19, 20] and the X-HALE aircraft [21]. The verification test case and its simulation results for the GTA model combining nonlinear flight dynamics and linearized structural dynamics are detailed in Section IV.A. Similar results for the X-HALE cases are presented in Section IV.B.

A. Load Alleviation Method Verification on GTA

1. GTA Model

The main GTA inertial and geometric parameters are summarized in Table 1. Sanghi et al. [20] established a beam-based model of GTA using the University Michigan's Nonlinear Aeroelastic Simulation Toolbox (UM/NAST) ([25]). The UM/NAST model has been verified against an MSC Nastran model configured using beam-type structural elements and doublet-lattice aerodynamic model as illustrated in Figure 3. The body-fixed reference frame is defined in agreement with the conventional North-East-Down flight mechanics orientation. The geometrically nonlinear UM/NAST model has 333 states which accounts for the rigid-body motion and for the flexibility of the wings and the fuselage. In this work, to further reduce the model order, a GTA reduced-order model has been created based on combining the 6-DOF rigid flight dynamics, linear structure dynamics, and aerodynamics linearization from UM/NAST model.

Table 1 General transport aircraft characteristics [19, 20]

Inertial properties (undeformed)		Geometric properties	
Mass (kg)	7.14×10^3	Wing span (m)	19
CG x-position (m)	0.46	Wing chord (m)	2.2
CG y-position (m)	0.00	Horizontal tail span (m)	8
CG z-position (m)	−0.97	Horizontal tail chord (m)	2.2
Roll inertia about CG (kg·m^2)	6.06×10^4	Vertical tail span (m)	6
Pitch inertia about CG (kg·m^2)	3.78×10^5	Vertical tail chord (m)	2.2
Yaw inertia about CG (kg·m^2)	3.82×10^5	Total aircraft length (m)	22

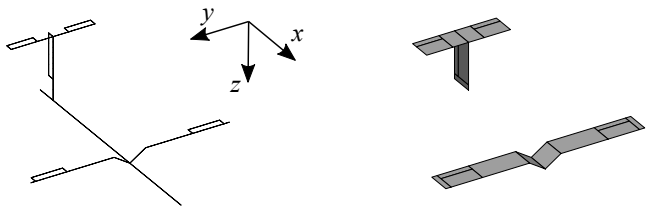

(a) Finite element model with beam element

(b) Doublet-lattice method aerodynamics model

Fig. 3 General transport aircraft modeling in MSC Nastran [19, 20]

The reduced-order model thus contains both states representing rigid-body motion and flexible responses of dominant modes. The rigid-body states contain the translational velocity $V = \{V_x, V_y, V_z\}^\top$ and rotational velocity components $\omega = \{p, q, r\}^\top$ (*i.e.*, roll, pitch, and yaw rates) of the body-fixed frame with respect to the ground frame expressed in the body-fixed frame, as well as the 3-2-1 Euler angles (*i.e.*, ϕ, θ, and ψ) representing the orientation of the body-fixed frame relative to the ground frame. The rates of the Euler angles relate to the angular velocity

$$\frac{d}{dt}\begin{Bmatrix}\phi\\ \theta\\ \psi\end{Bmatrix} = \underbrace{\begin{bmatrix}1 & \sin(\phi)\tan(\theta) & \cos(\phi)\tan(\theta)\\ 0 & \cos(\phi) & -\sin(\phi)\\ 0 & \frac{\sin(\phi)}{\cos(\theta)} & \frac{\cos(\phi)}{\cos(\theta)}\end{bmatrix}}_{R(\phi,\theta)}\omega. \tag{28}$$

The flexible states contain the modal amplitude of the first n_η dominant modes and their rates, written as η and $\dot{\eta}$, respectively. Therefore, the complete state x is written as

$$x = \{V^\top, \omega^\top, \eta^\top, \dot{\eta}^\top, \phi, \theta, \psi\}^\top. \tag{29}$$

The n_u-dimensional control input u contains both the thrust force and control surface deflections. The nonlinear flight dynamics in Eq. (13) is written in its equivalent format

$$E(x)\dot{x} = f_E(x) + g_E(x)u, \tag{30}$$

where

$$f_E(x) = E(x)f(x),\ g_E(x) = E(x)g(x). \tag{31}$$

The terms $E(x)$, $f_E(x)$ and $g_E(x)$ can be obtained from a VFA low-order model [26].

Table 2 Elastic modes of GTA obtained from the high-order UM/NAST model

Mode	Frequency (Hz)	Description
1	1.45	First bending mode of the right wing
2	1.45	First bending mode of the left wing
3	8.13	Second bending mode of the right wing
4	8.13	Second bending mode of the left wing

2. GTA Test Case Description

The GTA is trimmed at a cruise flight at an altitude of 6,096 m and speed of 160 m/s. At this flight condition, the trimmed angle of attack is 1.345°. To keep a relatively low-order system, four dominant modes are preserved (*i.e.*, $n_\eta = 4$) and they are listed in Table 2. Therefore, altogether, the model G contains a total of 17 states, including 9 rigid-body states and 8 flexible states (*i.e.*, η and $\dot{\eta}$).

The forward speed V_x and the pitch rate q are selected as the rigid-body outputs to the be controlled, *i.e.*,

$$y_r = \{V_x, q\}^\top. \tag{32}$$

To control the longitudinal dynamics, the 3-dimensional control input is specified as

$$u = \{F_T, \delta_E, \delta_A\}^\top, \tag{33}$$

where F_T is the thrust force, while δ_E and δ_A are the grouped elevator and aileron deflections, respectively. Note that both the ailerons and the elevators are also grouped symmetrically to only affect the longitudinal dynamics. The downward deflections are defined to be positive for both δ_E and δ_A. Note that $n_u = 3$ and $n_r = 2 < n_u$ indicate that the condition of weak input redundancy in Eq. (15) is satisfied. This redundancy is thus used to control an additional DOF. For MLA purposes, the first wing symmetric bending mode (*i.e.*, the mode composed of the first two half-wing out-of-plane bending modes with frequency 1.45 Hz) is identified to be the most significant flexible mode during longitudinal excitation. Thus, this mode is selected to be the flexible output to be controlled, *i.e.*,

$$y_f = \eta_1. \tag{34}$$

We employ a normalization to this mode shape so to keep it dimensional (units of meters) such that the (non-dimensional) unit modal amplitude, $\eta_1 = 1$, corresponding to a upward tip deflection of 0.11 m. For the given flight condition, the trimmed value of this mode equals 14.62, therefore, the initial condition satisfies $y_f(0) = 14.62$. In this application, the bounds on y_f are specified as

$$y_f^- = -25,\ y_f^+ = 25. \tag{35}$$

With this specification of inputs and outputs, the relative orders of the rigid-body states and the flexible states are given by $\rho_1 = \rho_2 = 1$ and $\rho_3 = 2$, respectively. Therefore, the designed trajectory of flexible outputs, $\tilde{y}_f(t), 0 \le t \le T$, should be at least twice continuously-differentiable.

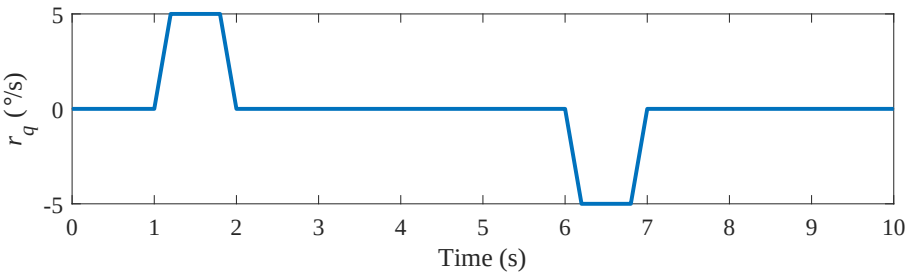

Fig. 4 Pitch rate reference trajectories of GTA

The reference trajectory of the pitch rate, r_q, is shown in Figure 4. The forward velocity is expected to be kept constant at 160 m/s during the climb maneuver. A rate-limited pitch-up maneuver of 4° is commanded for $t \in [1, 2]$ with a maximum rate of 5 degrees per second. A pitch-down maneuver is commanded for $t \in [6, 7]$ to bring the pitch angle back. The load factor during the pitch up maneuver is expected to be large due to the increased load factor. The MLA algorithms are most likely to affect the responses around this time range.

The feedback controller C adopted in this test case is a decoupled proportional-integral (PI) controller, where the forward speed V_x is regulated by the thruster input F_T while the pitch rate q is controlled by the grouped elevator deflection δ_E. The grouped symmetric aileron input δ_A is not used by this nominal controller C. The Laplace domain expression of the controller is written as

$$F_T(s) = (K_{p1} + K_{i1}/s)(r_{V_x}(s) - V_x(s)); \tag{36}$$

$$\delta_E(s) = -(K_{p2} + K_{i2}/s)(r_q(s) - q(s)); \tag{37}$$

$$\delta_A = 0, \tag{38}$$

where the gains are tuned and provided in Table 3. Note that Eq. (37) contains a negative sign, which arises from the fact that positive (downwards) elevator deflection yields a negative pitch rate (pitch down).

Table 3 Gains of nominal controller C for GTA

K_{p1} $(\mathrm{kN \cdot s \cdot m^{-1}})$	K_{i1} $(\mathrm{kN \cdot m^{-1}})$	K_{p2} (s)	K_{i2}
46	911	5	100

3. Performance of the MLA Method in the GTA Test Cases

The prediction and design of the responses of the flexible outputs are shown in Figure 5. As expected, the maximum $\hat{y}_f(t)$ arises at the pitch-up portion of the trajectory and it exceeds the prescribed upper bound y_f^+. Figure 2 shows the saturated $\bar{y}_f$ is generated by modifying $\hat{y}_f(t)$ when it violate the upper bound y_f^+ per Eq. (19). The saturated $\bar{y}_f(t)$ is further smoothed to get $\tilde{y}_f(t)$ which is twice continuously-differentiable. The smoothing is achieved through the identification of the saturation-induced switching time instants, followed by local smoothing around these switching points with zero-phase filters.

The nominal outputs and the outputs with the proposed MLA approach are shown in Figure 6. The forward speed V_x is kept within 0.1 m/s variations with the nominal controller. The roll rate q is also controlled to follow the reference provided in Figure 4 with less than 5% overshoot and without steady-state error. Due to the decoupling design, the proposed MLA method achieves an unchanged rigid-body response comparing to the nominal controller C. The identical rigid-body responses benefit from the input redundancy of the system. It also significantly simplifies the generation of the feedforward control signal Δu for MLA purpose, since the nominal control signal u_0 and rigid-body output y_r are not affected by Δu. The response of the flexible output agrees with its nominal predictions and designed modifications specified in Figure 5.

The control time histories with the nominal controller C only and the control time histories after the augmentation with the MLA signal are shown in Figure 7. The oscillations of the thrust force F_T during the pitch-up and pitch-down

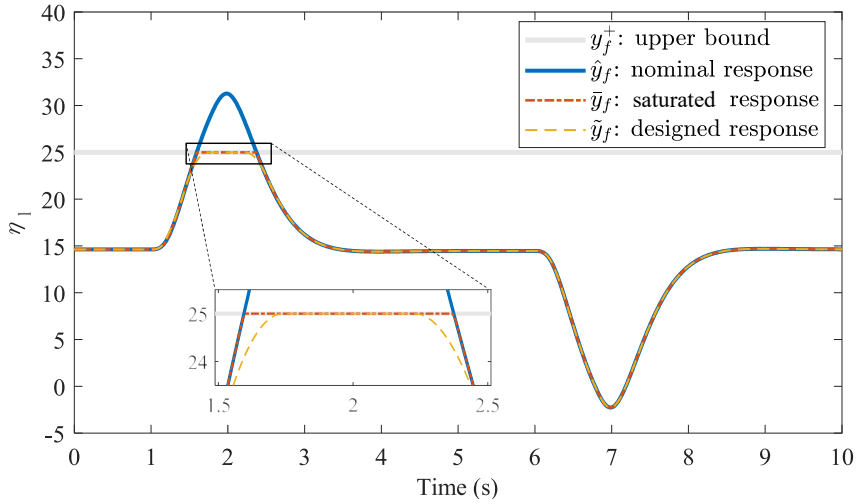

Fig. 5 GTA flexible outputs according to prescribed bounds

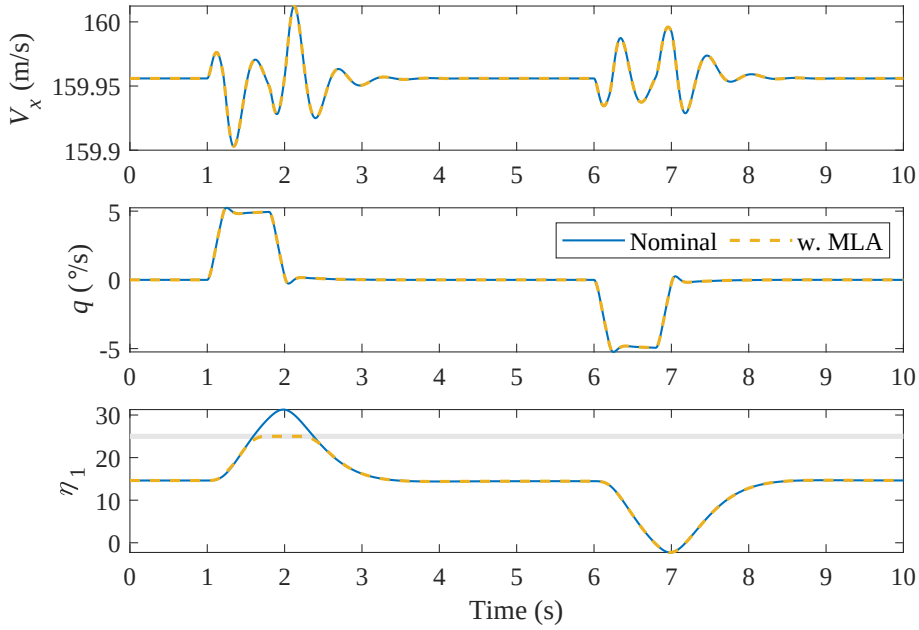

Fig. 6 GTA forward speed, pitch rate, and first symmetric bending modal amplitude with and without maneuver load alleviation

maneuvers arise from the coupling of the translational and rotational longitudinal flight dynamics. Note that almost twice the thrust force is required in the climb phase to maintain the speed constant. The grouped elevator input δ_E decreases at $t \in [1, 2]$ s, resulting in a positive pitching moment and a pitch-up response following the given trajectory. The input of δ_E has an opposite trend at $t \in [6, 7]$ s, which leads to a pitch-down maneuver. With the proposed MLA, parts of the control input of δ_E is shifted to δ_A around the time span where $\tilde{y}_f$ differs from $\hat{y}_f$. Note that with MLA the change of δ_E is small relative to δ_A. This is attributed to δ_E being more effective in controlling the pitching moment (compared to δ_A) due to its longer distance from the center of mass.

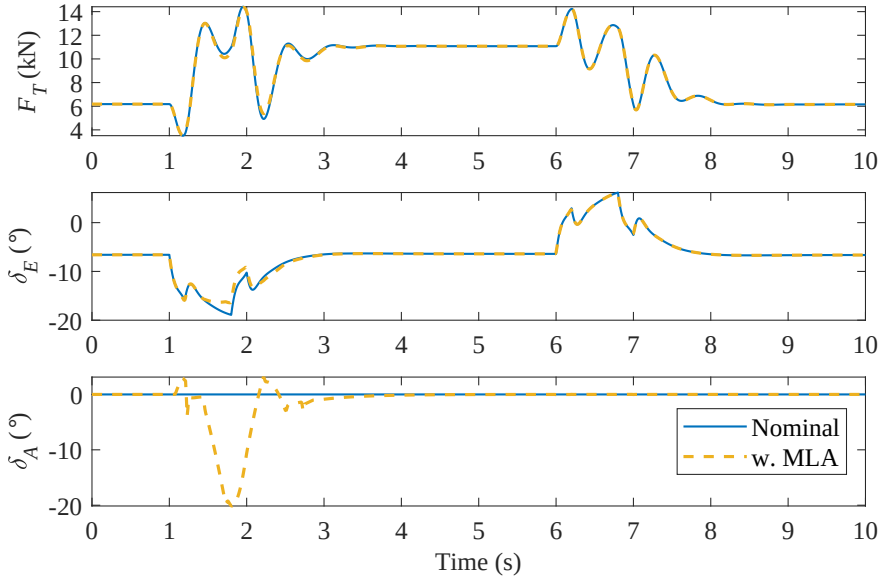

Fig. 7 GTA control inputs with and without maneuver load alleviation

B. Load Alleviation Method Verification on X-HALE

1. X-HALE Model

The X-HALE [21] is a very flexible unmanned aircraft developed at the University of Michigan for aeroelastic and control tests (Figure 8). The inertial and geometric properties of X-HALE are summarized in Table 4. In this work, a reduced-order model of the X-HALE, combining the 6-DOF rigid flight dynamics, linear structure dynamics, and aerodynamics linearization, is used. The reduced-order model is established following the same procedure as described in Section IV.A.1. Euler angles are adopted and their dynamics are given in Eq. (28).

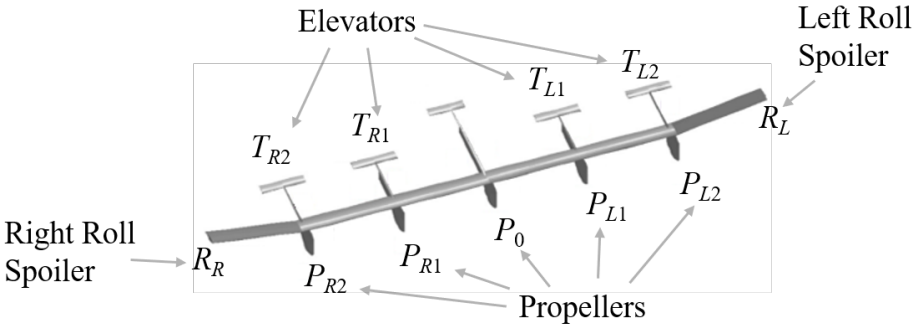

Fig. 8 Schematics of X-HALE

The X-HALE control inputs and their location are illustrated in Figure 8. The X-HALE is equipped with eleven all-movable control effectors (*i.e.*, $n_u = 11$), including four elevators ($T_{L1}, T_{L2}, T_{R1}, T_{R2}$), two roll spoilers ($R_L, R_R$), and five thrusters ($P_0, P_{L1}, P_{L2}, P_{R1}, P_{R2}$). Accordingly, the control input u is defined as

$$u = \left\{ \begin{array}{ccccccccccc} R_L & R_R & T_{L1} & T_{L2} & T_{R1} & T_{R2} & P_0 & P_{L1} & P_{L2} & P_{R1} & P_{R2} \end{array} \right\}^\top, \tag{39}$$

where positive values of the four elevator inputs ($T_{L1}, T_{L2}, T_{R1}, T_{R2}$) indicate a downward trailing edge movement. The vector of rigid-body outputs to be controlled ($n_r = 6$) consists of the translational velocity V and roll, pitch, and yaw

angular rates, *i.e.*,

$$y_r = \left\{ \begin{array}{cccccc} V_x & V_y & V_z & p & q & r \end{array} \right\}^\top. \tag{40}$$

The first two modes of the aircraft are the out-of-plane bending modes on the left and right wings. Their natural frequencies for these two dominant modes are both 0.60 Hz. The modal amplitudes are defined as η_L and η_R, and they are specified to be the flexible output y_f, *i.e.*,

$$y_f = \left\{ \begin{array}{cc} \eta_L & \eta_R \end{array} \right\}^\top. \tag{41}$$

Positive values of η_L and η_R indicate upward tip deflections.

Table 4 X-HALE characteristics

Inertial properties (undeformed)		Geometric properties	
Mass (kg)	11.33	Wing span (m)	4.97
CG x-position (mm)	27.8	Wing chord (m)	0.2
CG y-position (mm)	−4.3	Outer dihedral angle (°)	10
CG z-position (mm)	38.2	Center tail span (m)	0.388
Roll inertia about CG (kg·m^2)	23.0	Left and right horizontal tail span (m)	0.48
Pitch inertia about CG (kg·m^2)	1.14	Horizontal tail chord (m)	0.11
Yaw inertia about CG (kg·m^2)	23.2	Airspeed range (m/s)	[11, 19]

2. X-HALE Test Case Description

The X-HALE is trimmed at a typical flight condition: altitude of 30 m and airspeed of 14 m/s. At this condition, the wings already present a significant elastic deformation. Accordingly, the out-out-plane modal amplitudes η_L and η_R equal to 0.41 and 0.42, respectively. These two modal amplitudes are not strictly the same due to the slight asymmetry of the aircraft. Four dominant modes are preserved (*i.e.*, $n_\eta = 4$) to reduce the system order. Therefore, altogether, the model G contains a total of 17 states of which 9 rigid-body states and 8 flexible states (*i.e.*, η and $\dot{\eta}$). Unlike the GTA examples in Section IV.A where only longitudinal flight dynamics is included, the simulation verification of the proposed MLA method on the X-HALE considers both the longitudinal and lateral dynamics. Therefore, both the translational and rotational velocities are selected to be part of the rigid-body output to be controlled as defined in Eq. (40). Following the definition of the control input in Eq. (39), the aircraft contains more control inputs than the rigid-body outputs to be controlled. Note that $n_u = 11$ and $n_r = 6 < n_u$, indicating that the condition of weak input redundancy in Eq. (15) is satisfied. Accordingly, this redundancy can be used to control the additional DOFs. For MLA purposes, the amplitudes of η_L and η_R are to be controlled within specified bounds given by

$$y_f^- = \begin{Bmatrix} -0.43 \\ -0.43 \end{Bmatrix}, \; y_f^+ = \begin{Bmatrix} 0.43 \\ 0.43 \end{Bmatrix}. \tag{42}$$

With this specification of input and outputs, the relative degree of the rigid-body states equals 1 (*i.e.*, $\rho_1 = \rho_2 = \cdots = \rho_6 = 1$) while the relative degree of the flexible states equals 2 (*i.e.*, $\rho_7 = \rho_8 = 2$). Therefore, the designed trajectory of flexible outputs, $\tilde{y}_f(t), 0 \le t \le T$, should be at least twice continuously-differentiable.

Two reference trajectories of rotational velocities are shown in Figure 9. The first maneuver is a climb maneuver where the translation velocities are commanded to stay at 14 m/s. A rate-limited climb maneuver is defined between $t \in [1, 2]$ s with a maximum rate of 2 degrees per second. A similar pitch-down maneuver is commanded at $t \in [6, 7]$ s to bring the pitch angle back. The second maneuver is a coupled longitudinal and lateral reference where additional command on the roll and yaw rates are specified. These additional roll and yaw rate reference trajectories are specified at $t \in [1, 2]$ s and $t \in [6, 7]$ s with maximum rates of 1 degree per second, representing a climb and turn maneuver.

The nominal controller C adopts the control structure modified from the ones in [16, 27], and is illustrated in Figure 10. Cascaded proportional/proportional-integral (P/PI) controllers are used to generate the demanded roll, pitch, and yaw moments (*i.e.*, τ_p, τ_q, and τ_r). The demanded moments τ_p, τ_q, and τ_r are defined in a way that their positive

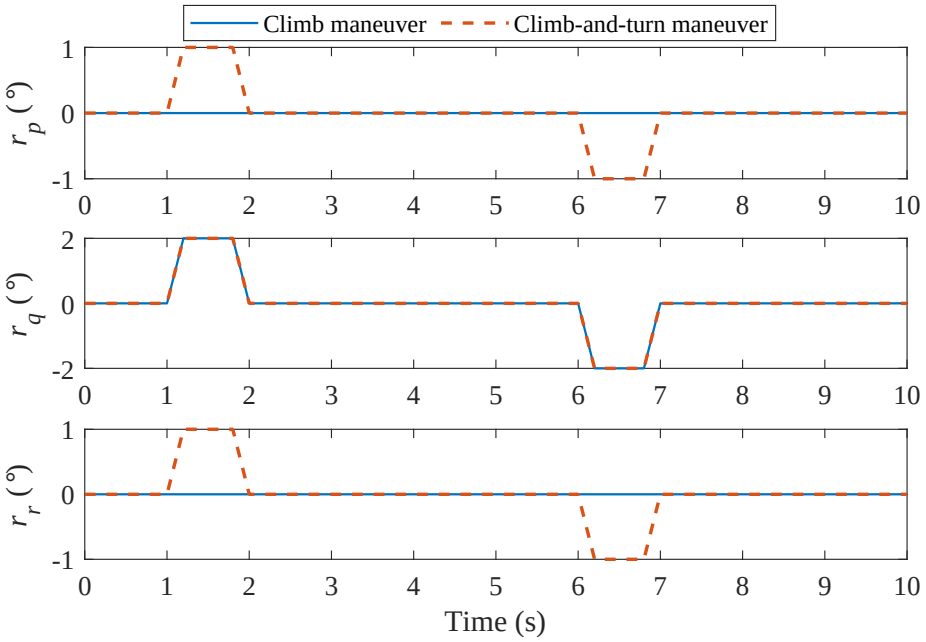

Fig. 9 Reference trajectories of the X-HALE maneuver

Table 5 Gains of the X-HALE nominal controller C

K_ϕ (s^{-1})	K_{pp} (s)	K_{pi}	K_θ (s^{-1})	K_{qp} (s)	K_{qi}	K_ψ (s^{-1})	K_{rp} (s)	K_{ri}	$K_{p,\text{tail}}$
1	0.15	0.1	15	0.01	0.2	1	0.5	5	0.8

values induce positive roll, pitch, and yaw motion, respectively. The corresponding gains are provided in Table 5. These demanded moments are further assigned to each control input as

$$
\begin{Bmatrix} R_L \\ R_R \end{Bmatrix} = \begin{cases} \begin{Bmatrix} R_{\max} & R_{R,\text{trim}} \end{Bmatrix}^\top & \text{if } \tau_p \le -\left(R_{\max} - R_{L,\text{trim}}\right) \\ \begin{Bmatrix} R_{L,\text{trim}} - \tau_p & R_{R,\text{trim}} \end{Bmatrix}^\top & \text{if } -\left(R_{\max} - R_{L,\text{trim}}\right) < \tau_p \le 0 \\ \begin{Bmatrix} R_{L,\text{trim}} & R_{R,\text{trim}} + \tau_p \end{Bmatrix}^\top & \text{if } 0 < \tau_p \le R_{\max} - R_{R,\text{trim}} \\ \begin{Bmatrix} R_{L,\text{trim}} & R_{\max} \end{Bmatrix}^\top & \text{if } R_{\max} - R_{R,\text{trim}} < \tau_p \end{cases}
$$

$$
\begin{aligned}
T_{L1} &= T_{R1} = \tau_q, \\
T_{L2} &= T_{\text{trim}} + \tau_q + K_{p,\text{tail}}\tau_p, \\
T_{R2} &= T_{\text{trim}} + \tau_q - K_{p,\text{tail}}\tau_p, \\
P_0 &= P_{\text{trim}}, \\
P_{L1} &= P_{L2} = P_{\text{trim}} + \tau_r, \\
P_{R1} &= P_{R2} = P_{\text{trim}} - \tau_r,
\end{aligned} \tag{43}
$$

where $R_{\max}$ is the maximum roll spoiler input amplitude, $R_{L,\text{trim}}$ and $R_{R,\text{trim}}$ are the trimmed left and right roll spoiler deflections, T_{trim} is the trimmed value of outer tail deflection, P_{trim} is the trimmed value of the propeller input, and $K_{p,\text{tail}}$ is the controller gain for differential outer tail deflections for enhanced roll authority. For X-HALE at the specified flight condition, $R_{\max} = 30°$, $R_{L,\text{trim}} = 0.5°$, $R_{R,\text{trim}} = 3.75°$, $T_{\text{trim}} = 1.19°$, and $P_{\text{trim}} = 84.12\%$. All the propeller input are scaled by its maximum continuous rotation speed 7, 200 rpm. Note that the spoiler inputs are asymmetrically defined for the roll motion with four different configurations considering different τ_p amplitudes. The inner tail control inputs (*i.e.*, T_{L1} and T_{R1}) are solely decided by the demanded pitch moment τ_q, while the outer tail control inputs (*i.e.*, T_{L2} and T_{R2}) are designed to provide additional roll actuation through asymmetrical deflections (regulated by the gain $K_{p,\text{tail}}$).

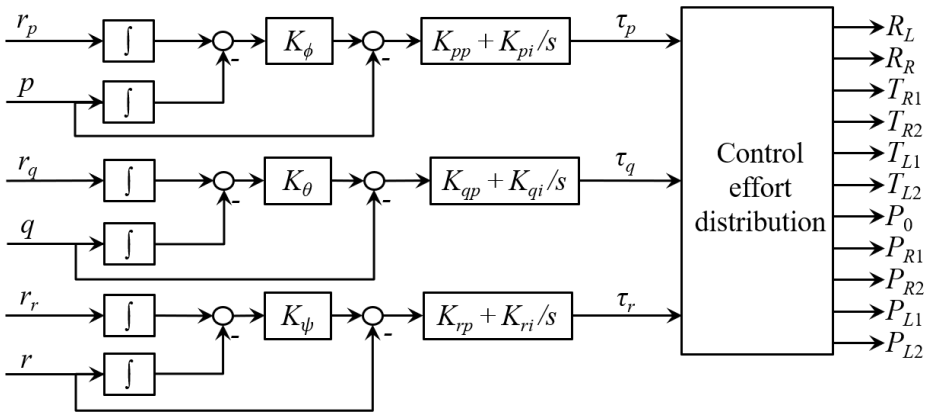

Fig. 10 Nominal controller C structure

3. Performance of the MLA Method in X-HALE Test Cases

The prediction and design of the responses of the flexible outputs for the climb maneuver is shown in Figure 11. The maximum $\hat{y}_f(t)$ arises at the pitch-up potion of the trajectory and it exceeds the prescribed upper bound y_f^+. Following the procedure described in Section III.B, the saturated $\bar{y}_f$ is generated by modifying the portion of $\hat{y}_f(t)$ which violate y_f^+. The saturated $\bar{y}_f(t)$ is further smoothed using moving average filters to get $\tilde{y}_f(t)$ that preserves second-order continuity. Note that two different smoothing time constants (T_{smooth}) are adopted here to generate $\tilde{y}_f(t)$.

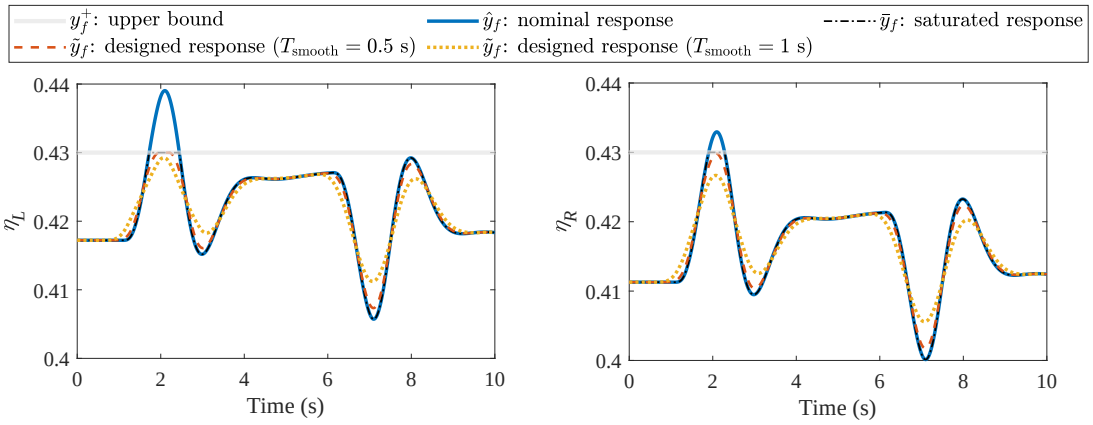

Fig. 11 Design of the flexible outputs of X-HALE according to prescribed bounds for the climb maneuver

The X-HALE responses to the climb maneuver, with and without the proposed MLA methods, are shown in Figure 12. With the nominal controller, the speed variations are within 0.3 m/s. The forward speed V_x is kept within 0.1 m/s variations with the nominal controller. Due to the slight asymmetry of the aircraft, this longitudinal climb maneuver still yields small roll and yaw responses. The pitch rate of 2°/s is well tracked with the nominal controller. Due to the input redundancy and nonlinear decoupling design, the new MLA method achieves an unchanged rigid-body response comparing to the nominal controller C. The responses of the flexible output, for both smoothing time constants, agree with its nominal predictions and designed modifications specified in Figure 11.

The control time histories with the nominal controller C only and the control signals after the augmentation with the MLA are shown in Figure 13. During the time when the load alleviation is active, the control effector inputs are altered to preserve the rigid-body responses while alleviating the root bending moment. Note that both the left and right roll spoilers are more intensively used at the instance where the load alleviation is mostly needed, indicating that the lift generated at the outer wings is reduced. At the same time, the inner and outer tail inputs (both left and right)

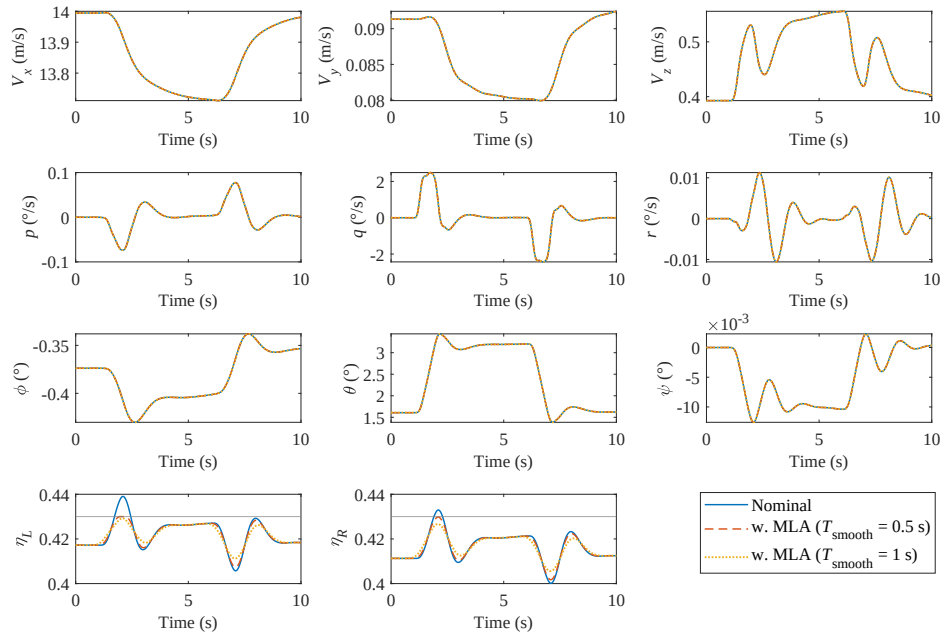

Fig. 12 X-HALE responses following the climb maneuver, with and without maneuver load alleviation

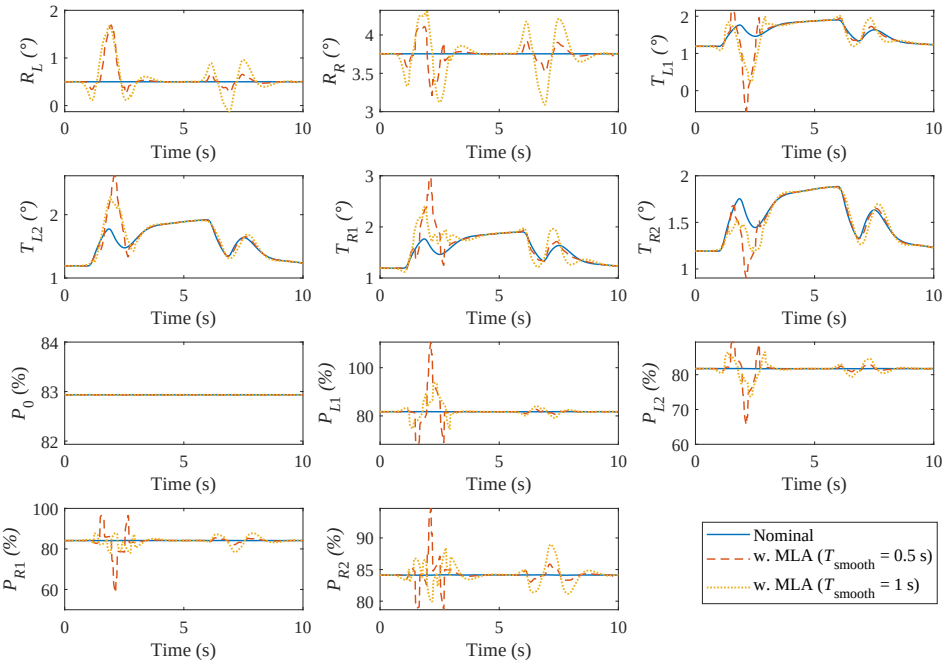

Fig. 13 X-HALE control input following the climb maneuver, with and without maneuver load alleviation

show complimentary modifications of its nominal values, indicating that the lift generated on the inner sections and the outer sections of the aircraft is redistributed. The amplitudes of the outer left tail T_{L2} significantly grows with the load violation of the nominal controller, indicating it is shifting the load inboard to alleviate the root moment. This is especially obvious for the left tails due to its relatively larger load violation on the left wing, as shown in Figure 11. The propellers are also modified with the MLA algorithm. Similar to the tail inputs, the MLA algorithm modifies the inner and outer propeller inputs in a complimentary way, such that the total propeller loads on the left and right wing do not vary with the load alleviation. Note that the trends of the propeller and the tail input modifications with the MLA method are shown to be opposite. These complimentary trends arise from the need to maintain a consistent total pitch moment with MLA, such that the rigid-body responses are invariant. With a relatively small smoothing time constant ($T_{\text{smooth}} = 0.5$ s), the propeller rpm may temporarily exceeds its specified maximum continuous value. This behavior is further reduced with the larger smoothing time constant (*e.g.*, control signals with MLA having $T_{\text{smooth}} = 1$ s in Figure 13).

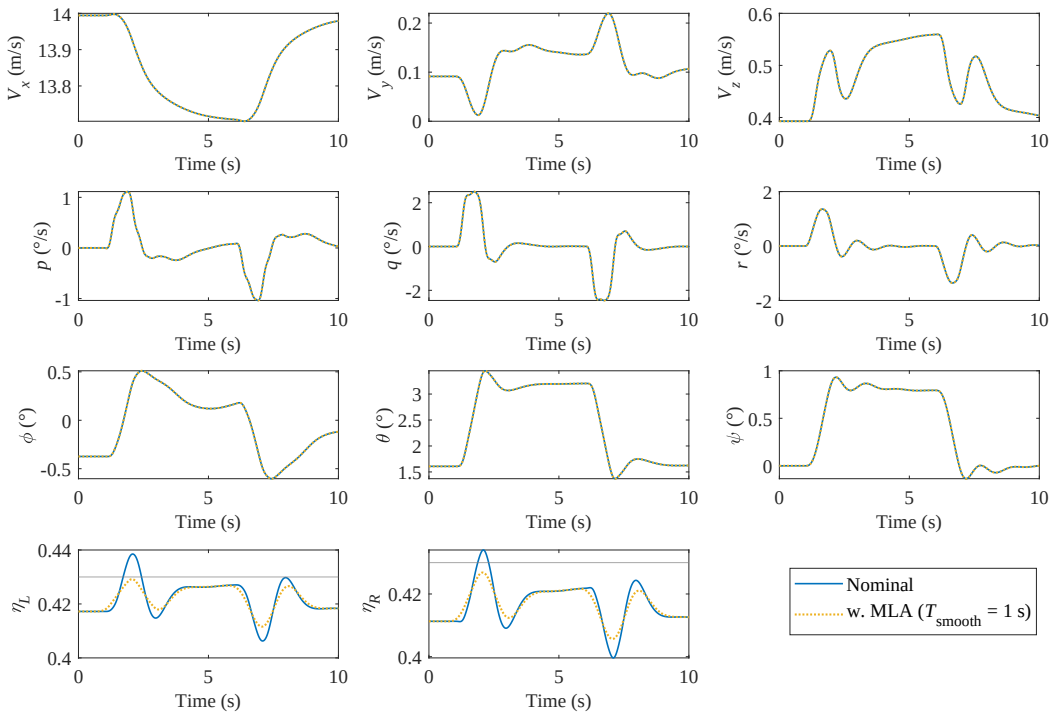

Fig. 14 X-HALE responses following the climb-and-turn maneuver, with and without maneuver load alleviation

Following the discussion of the X-HALE responses in Figure 12, the smoothing time constant $T_{\text{smooth}} = 1$ s is selected for the simulation of the climb-and-turn maneuver. The X-HALE responses to the climb-and-turn maneuver, with the nominal controller and with the proposed MLA methods, are shown in Figure 14. With the nominal controller, the reference roll, pitch, yaw rates are tracked. The wing deformation generated with this climb-and-turn maneuver is very similar to the climb maneuver, indicating that the longitudinal dynamics have a dominant influence on the dynamics of the modal amplitudes of the first out-of-plane bending modes (*i.e.*, η_L and η_R). Due to the input redundancy and nonlinear decoupling design, the proposed MLA method achieves an unchanged rigid-body response while alleviating the responses of the flexible responses.

The control signals to yielding this climb-and-turn maneuver, with and without the MLA functions, are shown in Figure 15. The trends of the roll spoiler input, tail input, and propeller input are similar to the ones shown in Figure 13. However, it is noticeable that the control input for this coupled longitudinal and lateral maneuver introduces more transients. This arises from the fact that the current designed flexible response $\tilde{y}_f$ only considers the satisfaction of the load bounds and the second-order continuity. To encourage the flexible responses to best approach the designed

response, the load alleviation function exploits the dynamics of the aircraft to reduce the load.

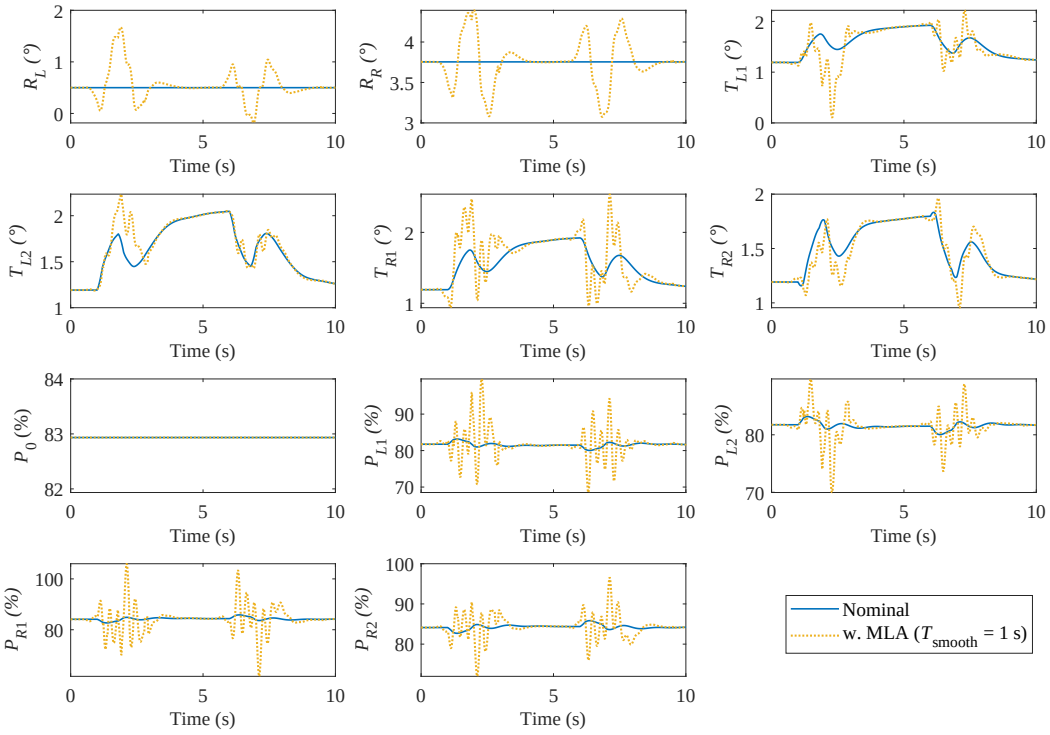

Fig. 15 X-HALE control input following the climb-and-turn maneuver, with and without maneuver load alleviation

V. Conclusion

This paper presented a maneuver load alleviation method for very flexible aircraft exploiting input redundancy. The method applies to geometrically nonlinear very flexible aircraft models with more control inputs than the rigid-body outputs. The input redundancy and nonlinear input-output decoupling principles enable the flexible outputs to be controlled separately from the rigid-body outputs. To achieve MLA, an additional feedforward control signal is added to the nominal controller output to alleviate the root bending moment. Using the prediction of the flexible outputs and its smoothed redesign satisfying the prescribed bounds, the feedforward control signal is generated exploiting the input-output decoupling. The proposed MLA method is verified in simulations of longitudinal maneuver of a very flexible general transport aircraft model, as well as the longitudinal and coupled maneuvers of the X-HALE unmanned aircraft model. The simulation case studies illustrate that the rigid-responses of the aircraft are kept unchanged while the first symmetric out-of-plane bending mode is alleviated as desired.

Acknowledgments

The authors would like to thank Prof. Moti Karpel (Technion) for proving the numerical model of the GTA used as the basis for the studies described here.

References

[1] Shearer, C. M., and Cesnik, C. E. S., "Nonlinear Flight dynamics of Very Flexible Aircraft," *Journal of Aircraft*, Vol. 44, No. 5, 2007, pp. 1528–1545.

[2] Silvestre, F. J., Guimarães Neto, A. B., Bertolin, R. M., da Silva, R. G. A., and Paglione, P., "Aircraft Control based on Flexible Aircraft Dynamics," *Journal of Aircraft*, 2017, pp. 262–271.

[3] Guo, S., Fu, Q., and Sensburg, O. K., "Optimal Design of a Passive Gust Alleviation Device for a Flying Wing Aircraft," *12th AIAA Aviation Technology, Integration, and Operations (ATIO) Conference and 14th AIAA/ISSM*, AIAA, Indianapolis, Indiana, 2012, p. 5625.

[4] Fonte, F., Toffol, F., and Ricci, S., "Design of a Wing Tip Device for Active Maneuver and Gust Load Alleviation," *2018 AIAA/ASCE/AHS/ASC Structures, Structural Dynamics, and Materials Conference*, 2018, p. 1442.

[5] Urnes, J., Nguyen, N., Ippolito, C., Totah, J., Trinh, K., and Ting, E., "A Mission Adaptive Variable Camber Flap Control System to Optimize High Lift and Cruise Lift to Drag Ratios of Future N+3 Transport Aircraft," *51st AIAA Aerospace Sciences Meeting including the New Horizons Forum and Aerospace Exposition*, 2013, p. 214.

[6] White, R. J., "Improving the Airplane Efficiency by Use of Wing Maneuver Load Alleviation," *Journal of Aircraft*, Vol. 8, No. 10, 1971, pp. 769–775.

[7] Burlion, L., Poussot-Vassal, C., Vuillemin, P., Leitner, M., and Kier, T., "Longitudinal Manoeuvre Load Control of a Flexible Large-scale Aircraft," *IFAC Proceedings Volumes*, Vol. 47, No. 3, 2014, pp. 3413–3418.

[8] Hashemi, K. E., and Nguyen, N. T., "Adaptive Maneuver Load Alleviation for Flexible Wing Aircraft with Nonminimum Phase Zeros," *2018 AIAA Guidance, Navigation, and Control Conference*, 2018, p. 619.

[9] Kopf, M., Bullinger, E., Giesseler, H.-g., Adden, S., and Findeisen, R., "Model Predictive Control for Aircraft Load Alleviation: Opportunities and Challenges," *2018 Annual American Control Conference (ACC)*, Milwaukee, USA, 2018, pp. 2417–2424.

[10] Pereira, M. d. F. V., Kolmanovsky, I. V., Cesnik, C. E. S., and Vetrano, F., "Model Predictive Control Architectures for Maneuver Load Alleviation in Very Flexible Aircraft," *AIAA Scitech 2019 Forum*, 2019, p. 1591.

[11] Zink, P. S., Mavris, D. N., and Raveh, D. E., "Maneuver Trim Optimization Techniques for Active Aeroelastic Wings," *Journal of Aircraft*, Vol. 38, No. 6, 2001, pp. 1139–1146.

[12] Raveh, D. E., "Maneuver Load Analysis of Overdetermined Trim Systems," *Journal of Aircraft*, Vol. 45, No. 1, 2008, pp. 119–129.

[13] Frost, S. A., Bodson, M., Burken, J. J., Jutte, C. V., Taylor, B. R., and Trinh, K. V., "Flight Control with Optimal Control Allocation Incorporating Structural Load Feedback," *Journal of Aerospace Information Systems*, Vol. 12, No. 12, 2015, pp. 825–835.

[14] Gaulocher, S. L., Roos, C., and Cumer, C., "Aircraft Load Alleviation During Maneuvers Using Optimal Control Surface Combinations," *Journal of Guidance, Control, and Dynamics*, Vol. 30, No. 2, 2007, pp. 591–600.

[15] Hansen, J. H., Duan, M., Kolmanovsky, I. V., and Cesnik, C. E. S., "Control Allocation for Maneuver and Gust Load Alleviation of Flexible Aircraft," *AIAA Scitech 2020 Forum*, 2020, p. 1186.

[16] Duan, M., Hansen, J. H., Kolmanovsky, I. V., and Cesnik, C. E. S., "Maneuver Load Alleviation of Flexible Aircraft through Control Allocation: A Case Study using X-HALE," *International Forum on Aeroelasticity and Structural Dynamics*, 2019, p. 109.

[17] Cesnik, C. E. S., Palacios, R., and Reichenbach, E. Y., "Reexamined Structural Design Procedures for Very Flexible Aircraft," *Journal of Aircraft*, Vol. 51, No. 5, 2014. doi:10.2514/1.C032464.

[18] Duan, M., and Okwudire, C., "Proxy-Based Optimal Control Allocation for Dual-Input Over-Actuated Systems," *IEEE/ASME Transactions on Mechatronics*, Vol. 23, No. 2, 2018, pp. 895–905.

[19] Karpel, M., Shousterman, A., Maderuelo, C., and Climent, H., "Dynamic Aeroservoelastic Response with Nonlinear Structural Elements," *AIAA Journal*, Vol. 53, No. 11, 2015, pp. 3233–3239.

[20] Sanghi, D., Riso, C., Cesnik, C. E. S., and Vetrano, F., "Impact of Control-Surface Flexibility on the Dynamic Response of Flexible Aircraft," *AIAA Scitech 2020 Forum*, 2020, p. 1185.

[21] Cesnik, C. E. S., Senatore, P. J., Su, W., Atkins, E. M., and Shearer, C. M., "X-HALE: A Very Flexible Unmanned Aerial Vehicle for Nonlinear Aeroelastic Tests," *AIAA journal*, Vol. 50, No. 12, 2012, pp. 2820–2833.

[22] Cheng, D., Hu, X., and Shen, T., *Analysis and design of nonlinear control systems*, Springer, 2010.

[23] McClamroch, N., and Schumacher, D., "An Asymptotic Output Tracking Problem for a Nonlinear Control System with Fewer Outputs than Inputs," *Proceedings of 32nd IEEE Conference on Decision and Control*, IEEE, 1993, pp. 3562–3563.

[24] Duan, M., and Okwudire, C. E., "Connections between Control Allocation and Linear Quadratic Control for Weakly Redundant Systems," *Automatica*, Vol. 101, 2019, pp. 96–102.

[25] Su, W., and Cesnik, C. E. S., "Nonlinear Aeroelasticity of a Very Flexible Blended-wing-body Aircraft," *Journal of Aircraft*, Vol. 47, No. 5, 2010. doi:10.2514/1.47317.

[26] Duan, M., Cesnik, C. E. S., Kolmanovsky, I. V., and Vetrano, F., "Nonlinear Low-order Modeling for Very Flexible Aircraft," *AIAA Scitech 2021 Forum*, 2021.

[27] Pang, Z. Y., "Modeling, Simulation and Control of Very Flexible Unmanned Aerial Vehicle," Ph.D. thesis, University of Michigan, Ann Arbor, 2018.